Electronic Supplementary Material (ESI) for Nanoscale Horizons.

SUPPORTING INFORMATION

Enhancement of exciton emission in WS_2 based on Kerker effect from the mode engineering of individual Si nanostripes

Jiahao Yan[1], Zhaoqiang Zheng[2], Zaizhu Lou[1], Juan Li[1], Bijun Mao[1], Baojun Li[1]*

1. Institute of Nanophotonics, Jinan University, Guangzhou 511443, China.

2. School of Materials and Energy, Guangdong University of Technology, Guangzhou 510006, China

*Corresponding author: baojunli@jnu.edu.cn

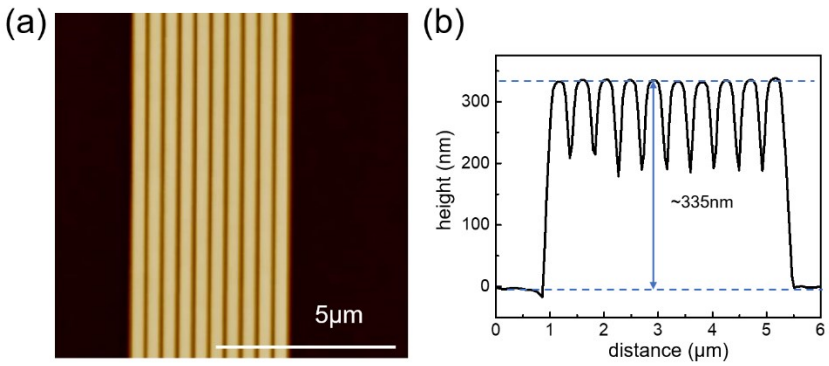

Figure S1. (a) An AFM image of the fabricated array of Si nanostripe. (b) The corresponding height profile.

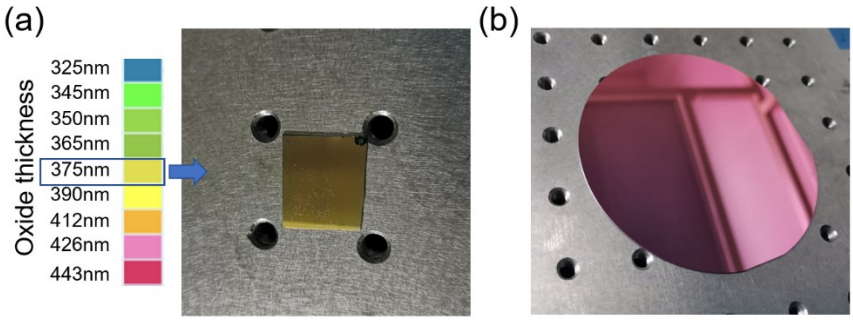

Figure S2. (a) A picture of fabricated sample, and the color chart of SiO_2 with different thicknesses on the Si substrate. The green-yellow color of the sample indicates the thickness of bottom oxide layer is exactly 375 nm. Therefore, redundant silicon was fully etched. (b) A picture of the purchased SOI wafer.

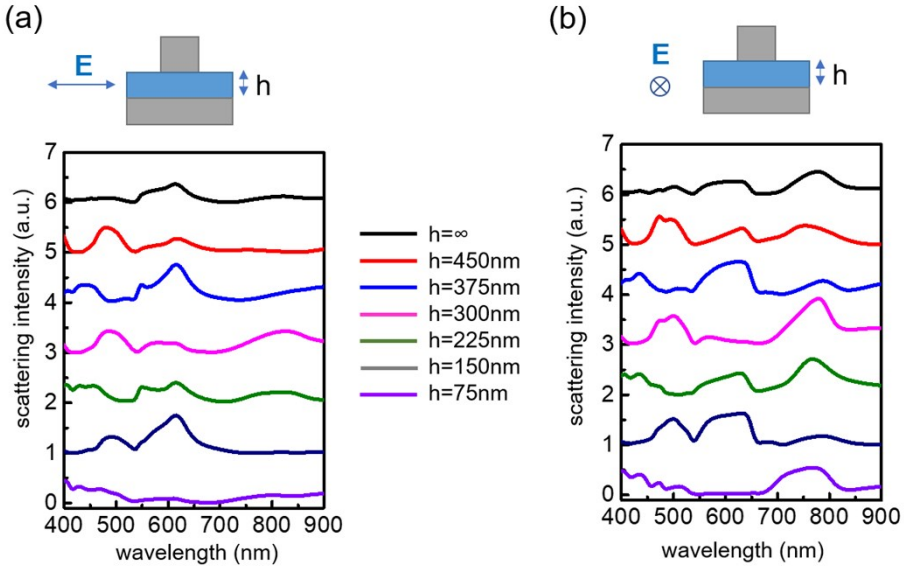

Figure S3. (a)(b) Simulated scattering spectra of the Si nanostripe with the width of 210 nm on bottom oxide layers with different thicknesses (h). Linear polarized incidence is perpendicular (a) or parallel (b) to the long axis of Si nanostripe.

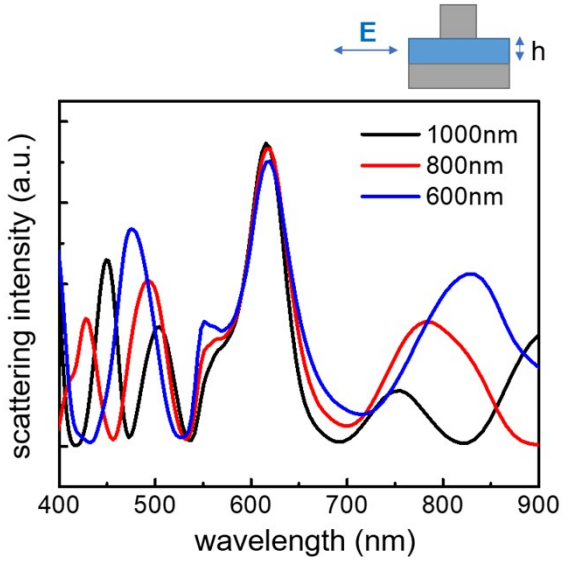

Figure S4. Simulated scattering spectra of the Si nanostripe with the width of 210 nm on bottom oxide layers with different thicknesses from 600 nm to 1000 nm. Linear polarized incidence is perpendicular to the long axis of Si nanostripe.

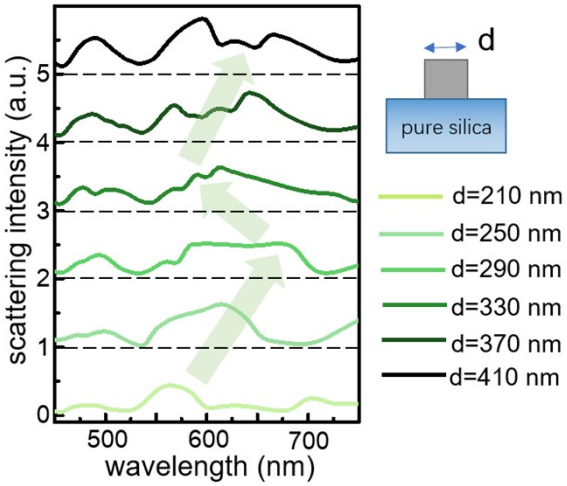

Figure S5. Width-dependent scattering spectra of the bare Si nanostripe on pure SiO_2 substrate. Unpolarized incident light was used.

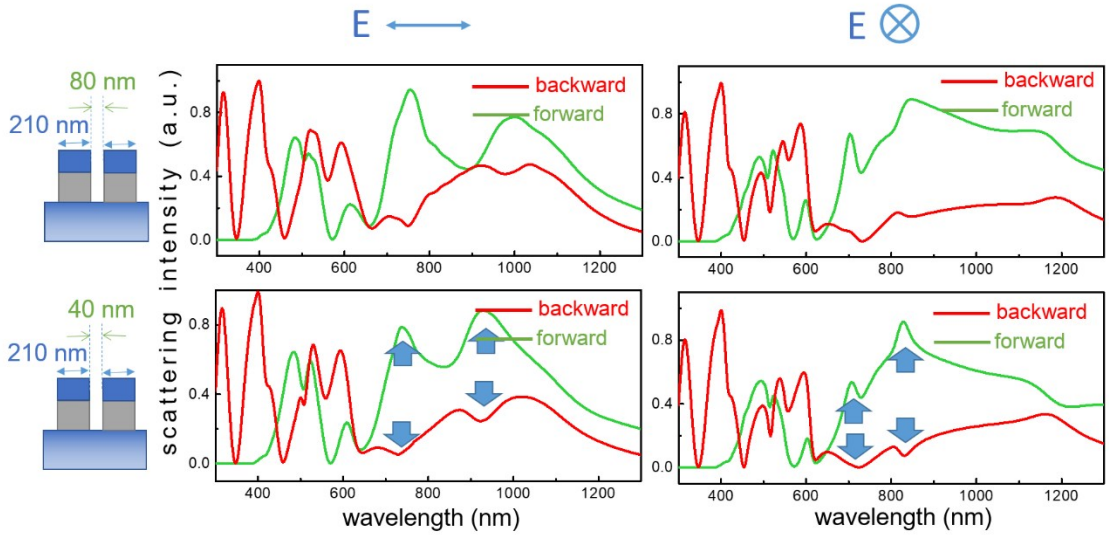

Figure S6. Simulated forward and backward scattering spectra of two kinds of Si nanostripe dimer (width: 210nm; gap distance: 80nm and 40 nm) under two orthogonal polarizations. Blue arrows showing the correspondence between dips and peaks.

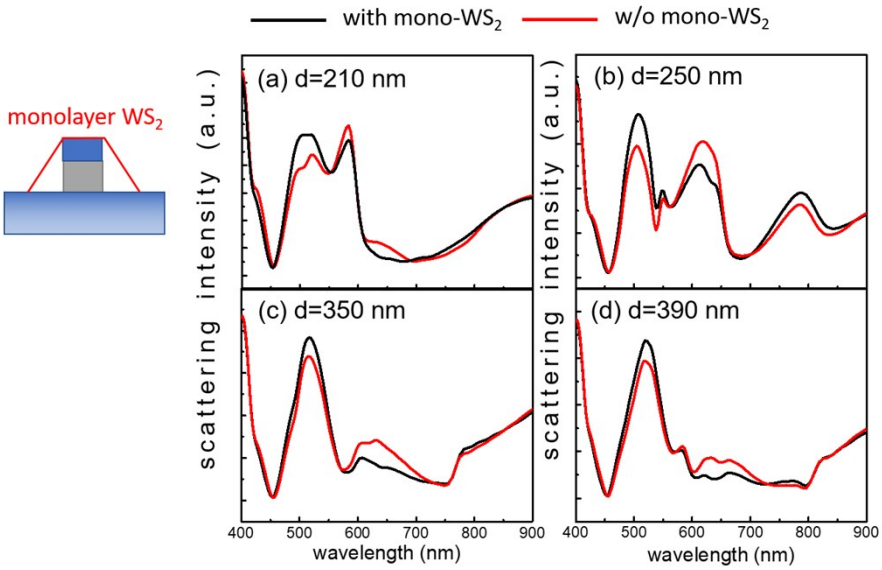

Figure S7. Simulated dark-field scattering spectra of Si nanostripes with and without monolayer WS_2 under unpolarized TFSF normal incidence.

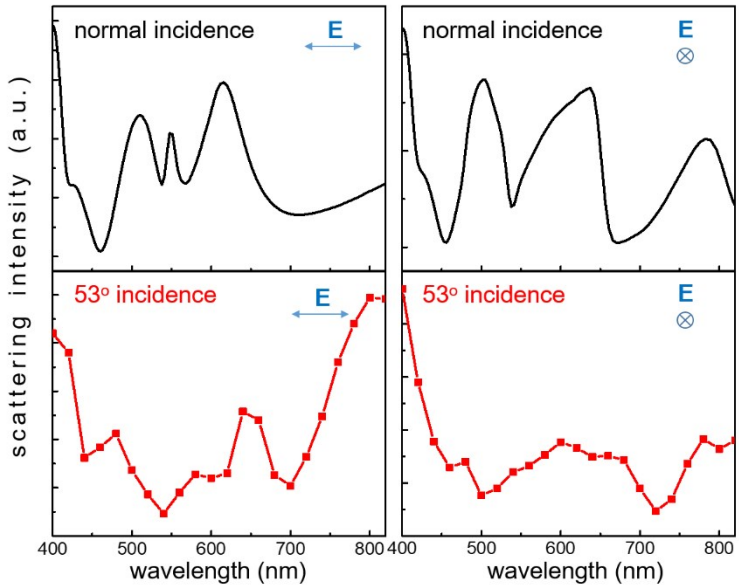

Figure S8. The comparison between simulated scattering spectra under normal incidence (black curves) and 53° oblique incidence (red curves) with two orthogonal polarizations.

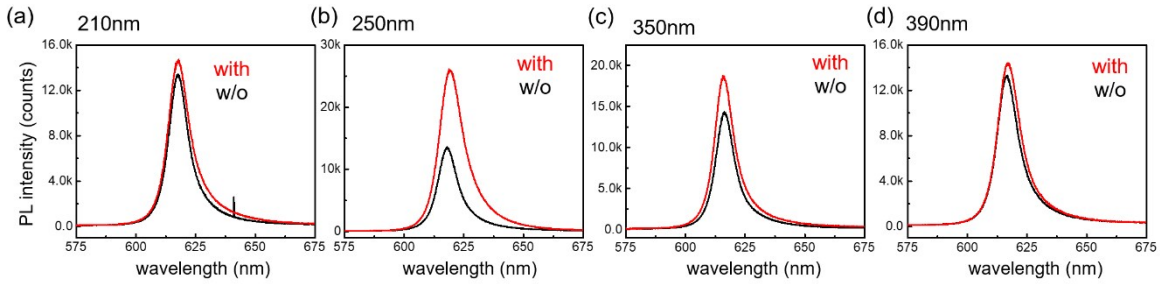

Figure S9. (a-d) PL spectra of monolayer WS_2 on Si nanostripes with widths of 210 nm (a), 250 nm (b), 350 nm (c) and 390 nm (d) compared with WS_2 on bottom SiO_2.

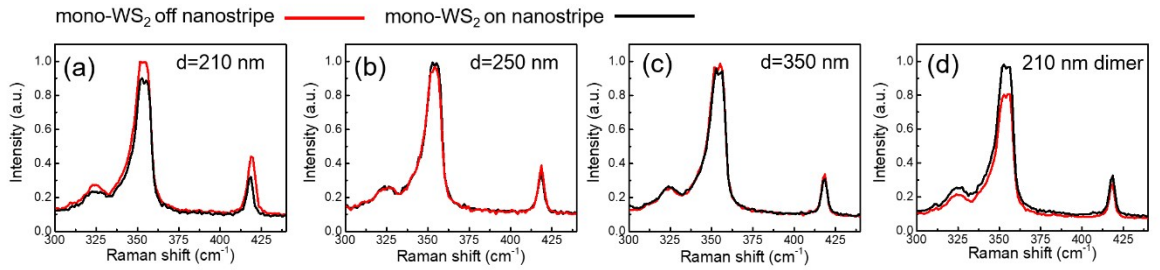

Figure S10. The Raman spectra measured on WS_2 monolayers with Si nanostripes (black curves) and without Si nanostripes (red curves) at exact locations where the PL were measured.

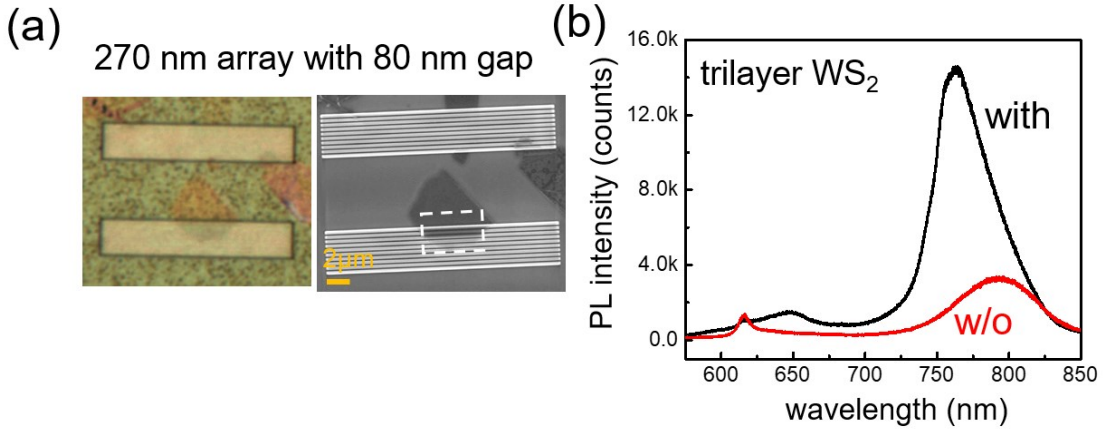

Figure S11. (a) Optical and SEM images of trilayer WS_2 on the 270 nm Si nanostripe array with the gap distance of 80 nm. The dashed box indicates the PL measurement region. (b) Measured PL spectra of the regions with or without WS_2 layers.

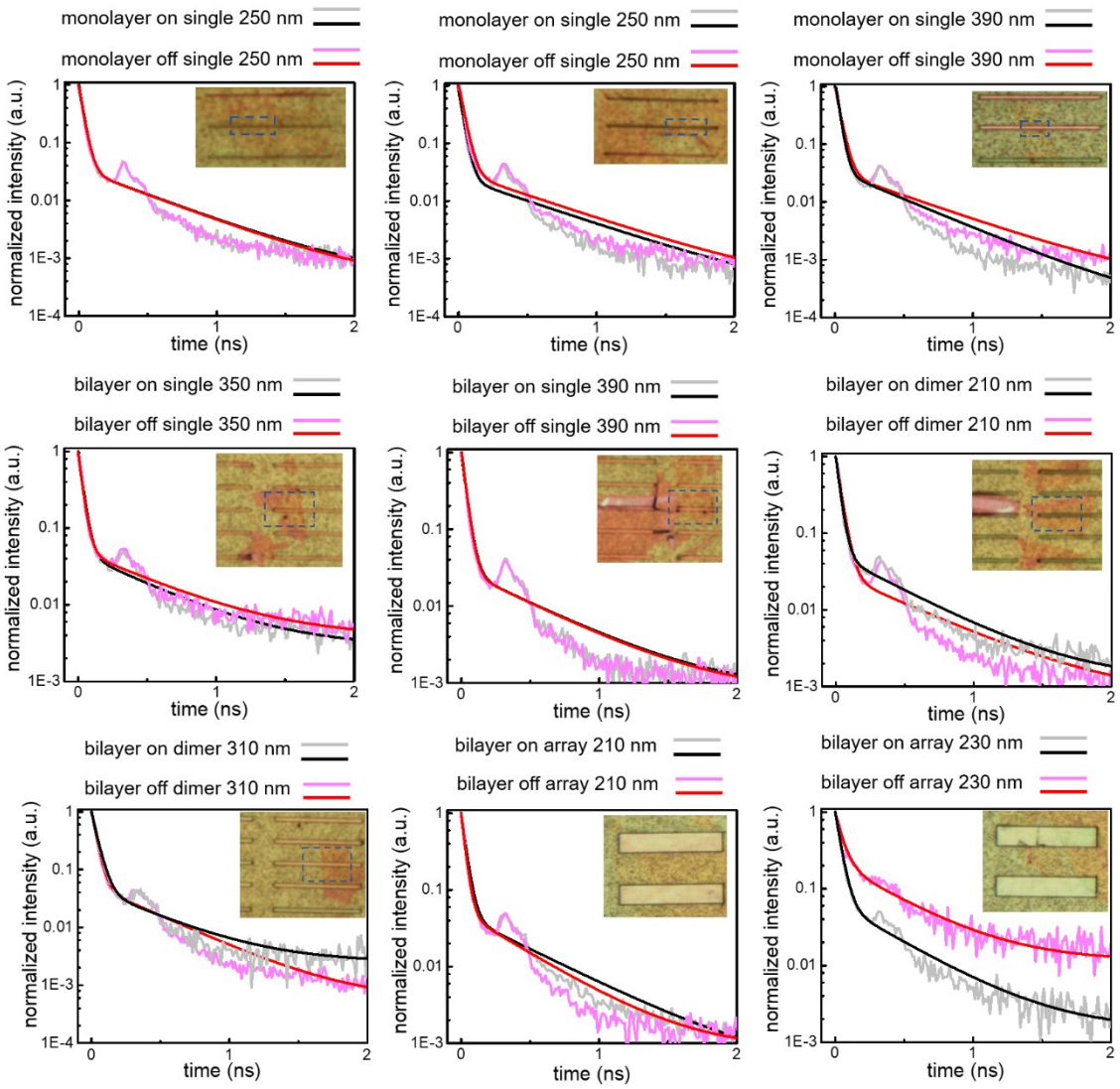

Figure S12. The time-resolved PL spectra of different locations (on nanostripes & off nanostripes) measured at the direct excitonic wavelengths. Insets are the optical images of the measured WS_2 flakes, which are the same samples measured in Fig. 3 and 4. All curves were fitted with the double-exponential function.

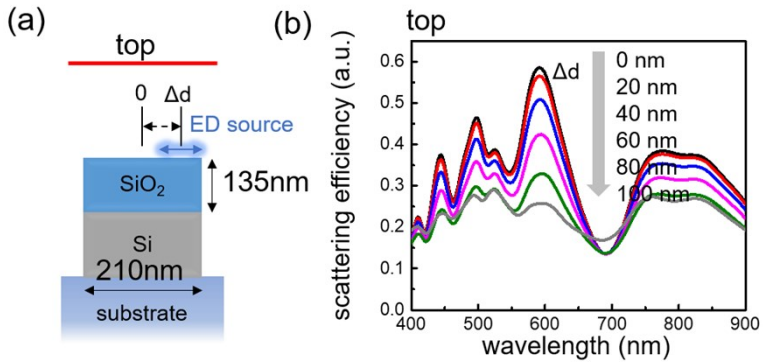

Figure S13. (a) Schematic showing the simulations based on the distance (Δd) between a dipole source and the center of nanostripe. (b) Simulated scattering efficiencies from dipole sources located at different positions.

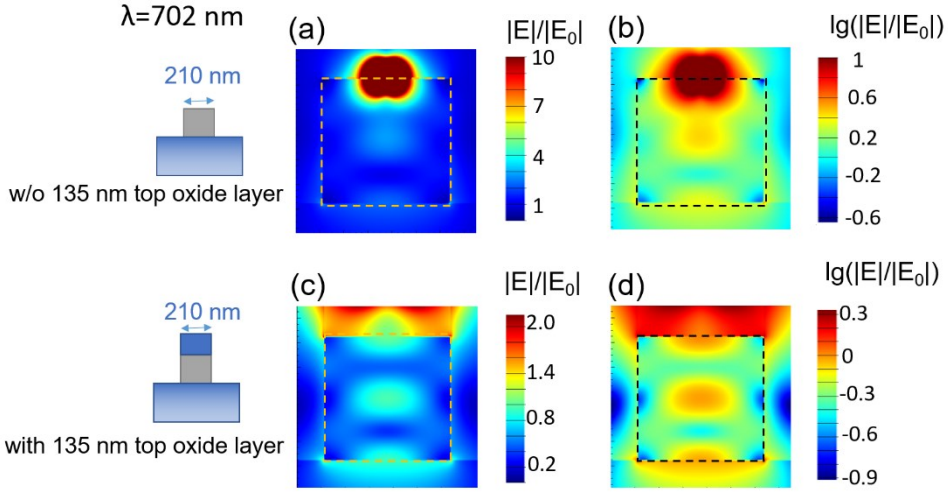

Figure S14. (a, b) Simulated electric field distributions under dipole source excitation at λ =702 nm. The dipole source contacts with the Si nanostripe directly. (c, d) Simulated electric field distributions under dipole source excitation at λ =702 nm. The dipole source and the Si nanostripe are separated by a 135 nm oxide layer. Dashed boxes indicate the cross section of the Si nanostripe.

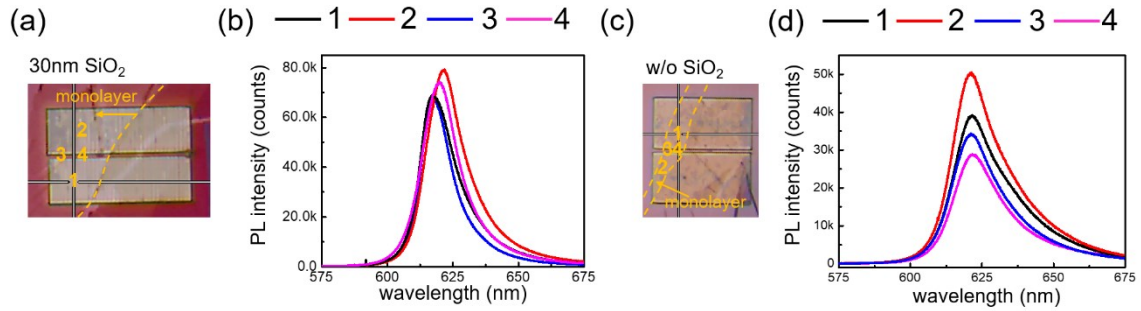

Figure S15. (a) The optical image of monolayer WS_2 on a fabricated Si nanostripe with 30 nm thick top oxide layer. The part of monolayer is labelled by the dashed line, and the numbers represent the test points. (b) PL spectra measured at each points. (c) The optical image of monolayer WS_2 on a fabricated Si nanostripe without top oxide layer. (d) PL spectra measured at each points.

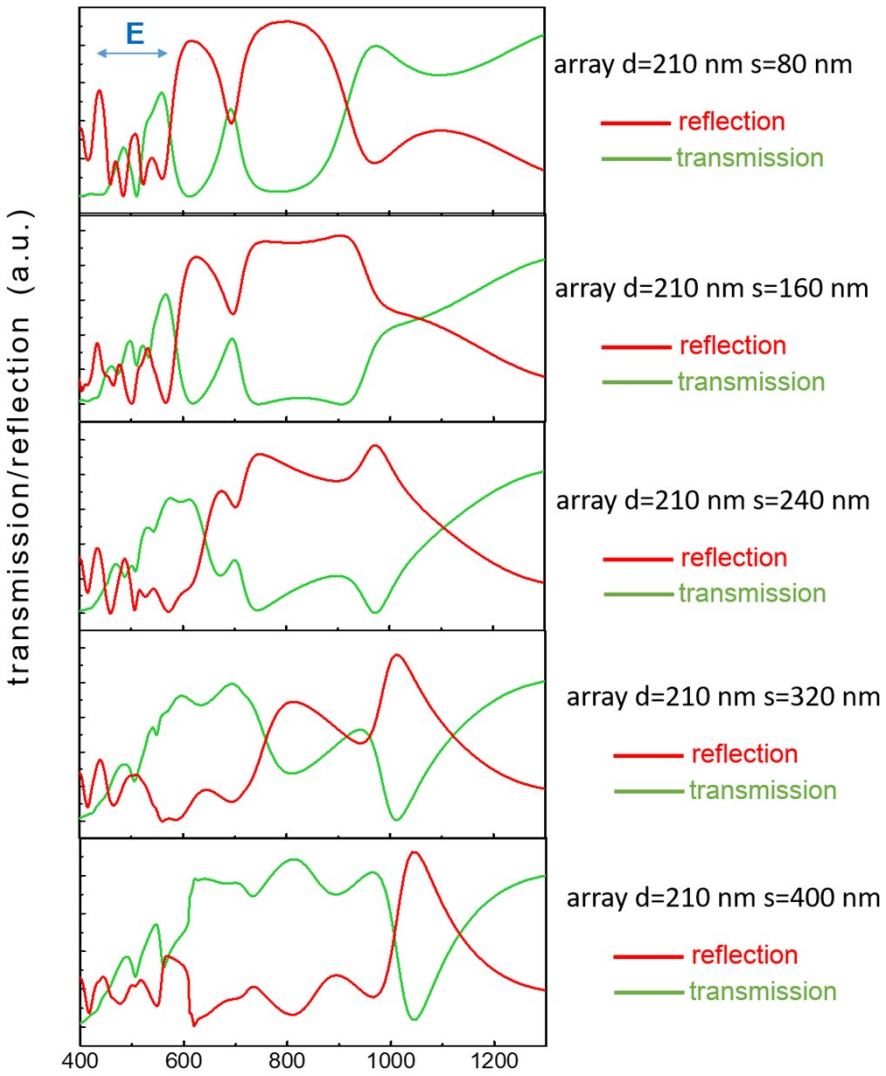

Figure S16. Simulated reflection and transmission spectra of Si nanostripe arrays with the width of 210 nm and the spacing of 80, 160, 240, 320 and 400 nm. Linear polarized incidence is perpendicular to the long axis of Si nanostripe.

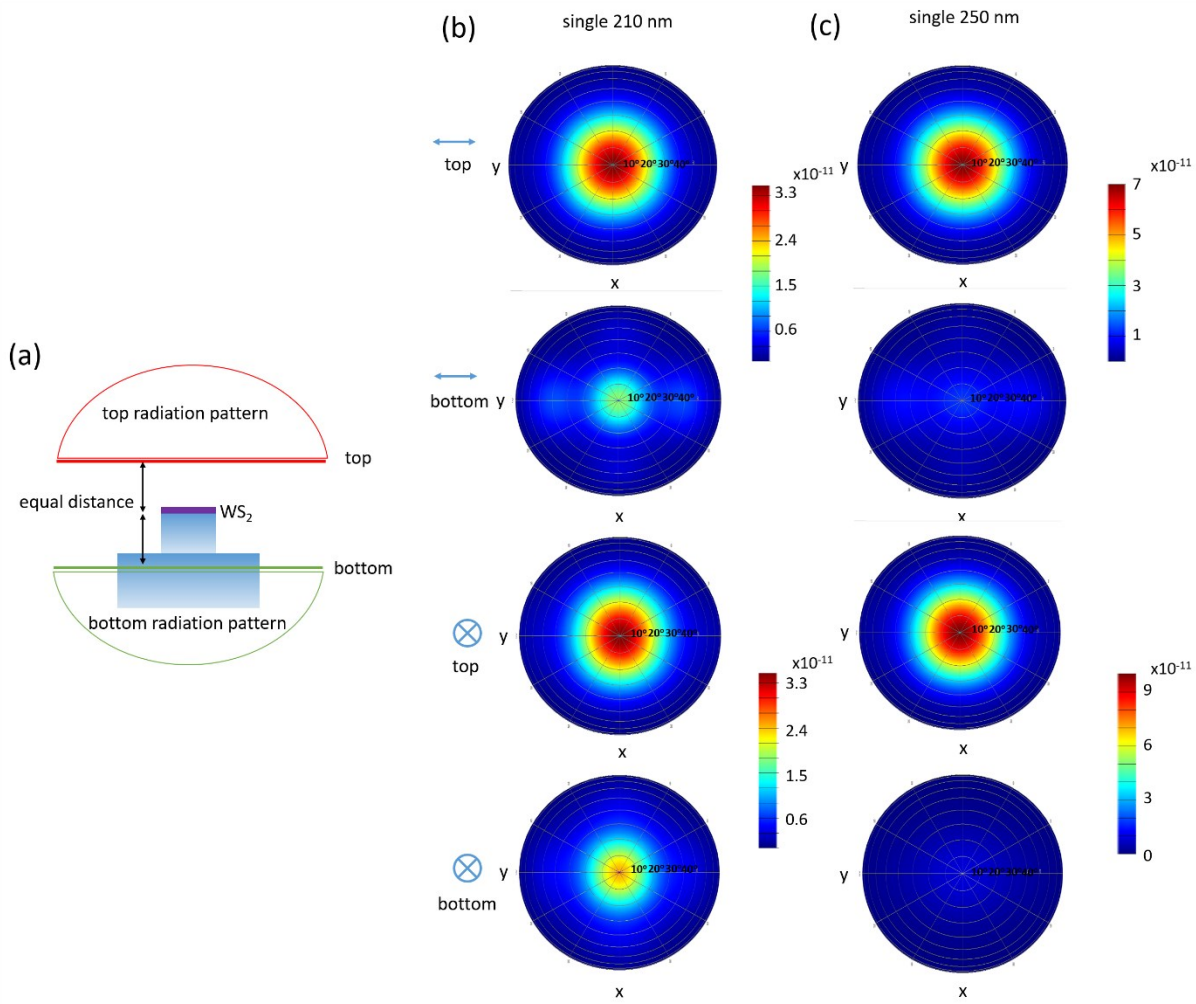

Figure S17. (a) Schematic showing the simulation of semi-spherical radiation patterns through top (detected direction in experiments) and bottom planar detectors. (b, c) Top and bottom radiation patterns of single Si nanostripes with the widths of 210 nm (b) and 250 nm (c) at the direct excitonic wavelength of WS_2 monolayers (618 nm). The polarization direction of dipole sources is perpendicular or parallel to the long axis of Si nanostripe. Values of divergence angle are labelled inside radiation patterns.

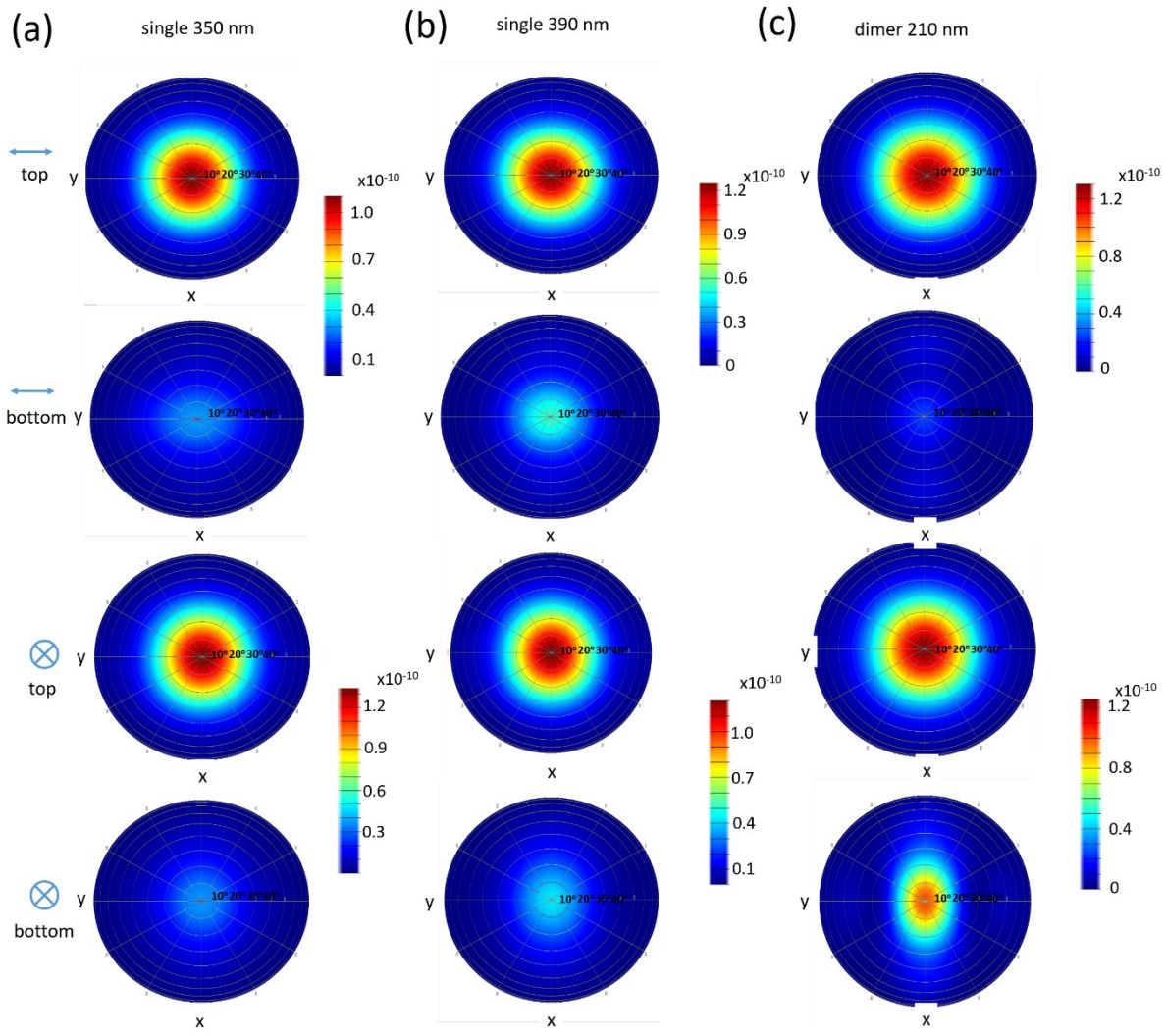

Figure S18. (a, b) Top and bottom radiation patterns of single Si nanostripes with the widths of 350 nm (a) and 390 nm (b) at the direct excitonic wavelength of WS_2 monolayers (618 nm). The polarization direction of dipole sources is perpendicular or parallel to the long axis of Si nanostripe. Values of divergence angle are labelled inside radiation patterns. (c) Top and bottom radiation patterns of a Si nanostripe dimer with the width of 210 nm and the gap of 80 nm.

Table S1. Calculations of the overall enhancement factors based on directivities, spot sizes, Purcell factors and the absorption at the excitation wavelength. All samples were studied at the direct excitonic wavelengths (618 nm for monolayers and 630 nm for bilayers). Average directional enhancement has considered the spot size (area ratio), directivity from WS_2 layers off nanostripes and two orthogonal polarizations. The average absorption enhancement also based on the same calculation process. Overall enhancement factors is the product of average directional enhancement factors, Purcell factors and average absorption enhancement factors.

Hybrid systems	PL enhancement factor	⟷ directivity	⊗ directivity	directivity without nanostripe	area ratio	average directional enhancement	Purcell factor	$\lvert E\rvert^2$ at 514 nm ⟷	$\lvert E\rvert^2$ at 514 nm ⊗	$\lvert E\rvert^2$ without nanostripe	average absorption enhancement	overall enhancement factor
210 nm single nanostripe & monolayer WS_2	1.1	1.4	1.2	0.54	0.247	1.347	0.983	2.098	1.491	1.809	0.998	1.322
250 nm single nanostripe & monolayer WS_2	1.9	2.4	5.6	0.54	0.294	2.884	1.05	2.252	2.290	1.809	1.075	3.256
350 nm single nanostripe & monolayer WS_2	1.3	2.3	2.5	0.54	0.412	2.418	1	2.001	1.225	1.809	0.955	2.310
390 nm single nanostripe & monolayer WS_2	1.07	2.1	2.1	0.54	0.459	2.325	0.983	1.734	1.016	1.809	0.889	2.036
210 nm nanostripe dimer & monolayer WS_2	2.85	3.6	1.4	0.54	0.588	3.135	1	1.719	1.150	1.809	0.878	2.753
210 nm single nanostripe & bilayer WS_2	0.97	1	1.3	0.57	0.247	1.251	1	2.098	1.491	1.809	0.998	1.249
350 nm single nanostripe & bilayer WS_2	2.28	2.3	2.5	0.57	0.412	2.322	1.158	2.001	1.225	1.809	0.955	2.570
390 nm single nanostripe & bilayer WS_2	2.18	2.1	2.6	0.57	0.459	2.432	0.985	1.734	1.016	1.809	0.889	2.132
210 nm nanostripe dimer & bilayer WS_2	2.61	1.2	1.9	0.57	0.588	2.011	1.045	1.719	1.150	1.809	0.878	1.846
310 nm nanostripe dimer & bilayer WS_2	3.83	3.8	3.6	0.57	0.824	5.522	1.104	1.738	1.179	1.809	0.840	5.128
210 nm nanostripe array & bilayer WS_2	2.55	2.1	1.8	0.57	1	3.421	1.029	1.286	0.767	1.809	0.567	2.000
230 nm nanostripe array & bilayer WS_2	9.44	5.7	3.2	0.57	1	7.807	1.913	0.816	0.706	1.809	0.420	6.286

Table S2. Comparison of the PL enhancement factors between our work and other works based on plasmonic or dielectric nanostructures.

Heterostructures (single nanoantennas)	PL enhancement factor	Non-radiative loss $\propto \varepsilon''(\lvert E\rvert/\lvert E_0\rvert)^2$	Heterostructures (arrays or other nanoantennas with "hot spots")	Enhancement factor $=\frac{I_{on}}{A_{structures}}\left(\frac{I_{off}}{A_{laser}}\right)^{-1}$
Si nanoparticles & monolayer WS_2[1]	0.1-0.6	10.4	Si_3N_4 gratings & monolayer WSe_2[7]	2 (300K)-7 (77k)
Si nanowire & monolayer MoS_2[2]	1.5-2.5	unknown	Si gratings & monolayer WSe_2[8]	1.3-3
Au nanoparticles & fewlayer MoS_2[3]	0.88-1.04	182	Si metasurfaces & monolayer MoS_2[9]	15-35
Tapered Au nanoantenna & monolayer MoS_2[4]	3.2	unknown	SiN photonic crystal & monolayer MoS_2[10]	1300
Au nanorods & monolayer WS_2[5]	4-6	1970	GaP dimer & monolayer WSe_2[11]	10000
Ag nanoantennas & monolayer MoS_2[6]	0.5-2	600	Au nanorod array & monolayer MoS_2[12]	1.65
Our work: Single Si nanostripes & mono- or bilayer WS_2	1-4	~0	Our work: Si nanostripe array & bilayer WS_2	9.5

References

1. C. Ma, J. Yan, Y. Huang and G. Yang, *Mater. Horiz.*, 2019, **6**, 97-106.
2. A. F. Cihan, A. G. Curto, S. Raza, P. G. Kik and M. L. Brongersma, *Nature Photon.*, 2018, **12**, 284.
3. J. Yan, C. Ma, P. Liu and G. Yang, *ACS Photon.*, 2017, **4**, 1092-1100.
4. E. Palacios, S. Park, L. Lauhon and K. Aydin, *ACS Photon.*, 2017, **4**, 1602-1606.
5. J. Kern, A. Trugler, I. Niehues, J. Ewering, R. Schmidt, R. Schneider, S. Najmaei, A. George, J. Zhang, J. Lou, U. Hohenester, S. M. de Vasconcellos and R. Bratschitsch, *ACS Photon.,* 2015, **2**, 1260-1265.
6. W. Gao, Y. H. Lee, R. Jiang, J. Wang, T. Liu and X. Y. Ling, *Adv. Mater.*, 2016, **28**, 701-706.
7. N. M. H. Duong, Z.-Q. Xu, M. Kianinia, R. Su, Z. Liu, S. Kim, C. Bradac, T. T. Tran, Y. Wan, L.-J. Li, A. Solntsev, J. Liu and I. Aharonovich, *ACS Photon.,* 2018, **5**, 3950-3955.
8. H. Chen, S. Nanz, A. Abass, J. Yan, T. Gao, D.-Y. Choi, Y. S. Kivshar, C. Rockstuhl and D. N. Neshev, *ACS Photon.*, 2017, **4**, 3031-3038.
9. T. Bucher, A. Vaskin, R. Mupparapu, F. J. F. Lochner, A. George, K. E. Chong, S. Fasold, C. Neumann, D.-Y. Choi, F. Eilenberger, F. Setzpfandt, Y. S. Kivshar, T. Pertsch, A. Turchanin and I. Staude, *ACS Photon.,* 2019, **6**, 1002-1009.
10. X. Zhang, S. Choi, D. Wang, C. H. Naylor, A. C. Johnson and E. Cubukcu, *Nano Lett.*,

2017, **17**, 6715-6720.

11. L. Sortino, P. G. Zotev, S. Mignuzzi, J. Cambiasso, D. Schmidt, A. Genco, M. Aβmann, M. Bayer, S. A. Maier, R. Sapienza and A. I. Tartakovskii, *Nat. Commun.,* 2019. **10**, 5119.

12. S. Najmaei, A. Mlayah, A. Arbouet, C. Girard, J. Leotin and J. Lou, *ACS Nano*, 2014, **8**, 12682-12689.